Timing and significance of maximum and minimum equatorial insolation

Yosef Ashkenazy[1] and Hezi Gildor[2]

Received 18 February 2007; revised 6 September 2007; accepted 27 September 2007; published 31 January 2008.

[1] Variations in summer insolation at high northern latitudes on a timescale of 100 ka are very small. Thus a common belief is that the pronounced ~100 ka glacial cycles are not directly linked to the very weak 100 ka insolation periodicity. Here we show, analytically and numerically, that the annual maximum (and minimum) of daily equatorial insolation has pronounced eccentricity periodicities, with timescales of ~400 ka and ~100 ka, as well as a pronounced half-precession periodicity with timescale of ~11 ka. The timing of the maximum (and minimum) annual equatorial insolation may change around the equinoxes (solstices), alternating between the vernal and autumnal equinoxes (summer and winter solstices) where the time of the maximum (minimum) equatorial insolation may occur up to more than 1 month from the equinoxes (solstices). We also show that when considering the mean insolation of periods larger than 1 d, the ~11 ka periodicity becomes less dominant, and it vanishes when the averaging period is half a year; for the later case the maximum (minimum) may occur for any day in the annual cycle. The maximum equatorial insolation may alter the timing and amplitude of the maximum surface temperature of the summer hemisphere and in this way may drastically affect the Hadley circulation. Changes in Hadley circulation affect the heat and moisture transport from low to high latitudes, affecting the buildup of the high-latitude Northern Hemisphere ice sheets.

Citation: Ashkenazy, Y., and H. Gildor (2008), Timing and significance of maximum and minimum equatorial insolation, *Paleoceanography*, *23*, PA1206, doi:10.1029/2007PA001436.

1. Introduction

[2] The most pronounced climate phenomena over the last 800 ka or so are glacial-interglacial oscillations, characterized by a 100 ka timescale [e.g., *Imbrie et al.*, 1984]. Traditionally, these oscillations have been attributed to changes in summer insolation at high northern latitudes, where much of the ice accumulated. The insolation for a given latitude and day in the annual cycle depends on the orbital parameters of eccentricity, obliquity, and precession [*Adhémar*, 1842; *Croll*, 1875; *Milankovitch*, 1941]. The basic idea was that summer insolation dictated whether snow falling during winter would survive melting during summer and accumulate [e.g., *Paillard*, 2001], although modifications have been proposed (e.g., *Huybers* [2006] has suggested that melting is primarily controlled by the number of ''degree days''). The orbital parameters have timescales of ~100 ka, ~40 ka, and ~20 ka respectively [*Milankovitch*, 1941; *Berger*, 1978; *Laskar*, 1990; *Laskar et al.*, 1993; *Rubincam*, 2004]. However, changes in high-latitude insolation on the 100 ka eccentricity frequency are too weak to explain the pronounced 100 ka periodicity of the glacial-interglacial oscillations [e.g., *Imbrie et al.*, 1993].

[3] There are many theories to explain glacial-interglacial oscillations. Most fit into one of the following categories: (1) Insolation variations drive glacial dynamics; without insolation forcing the model's glacial oscillations would not exist [e.g., *Berger and Loutre*, 1996; *Paillard*, 1998]. (2) Glacial-interglacial oscillations are due to internal dynamics of the climate system and would exist even without the insolation forcing [e.g., *Saltzman and Sutera*, 1984; *Saltzman*, 1987, 1990; *Gildor and Tziperman*, 2000; *Ashkenazy and Tziperman*, 2004]. According to the first approach the pronounced 100 ka periodicity of the glacial cycles is a result of nonlinear response of the climate system to changes in insolation. On the other hand, according to the second approach, the role of the Milankovitch forcing is to phase lock (i.e., set the timing) and modulate the internal, self-sustained, glacial cycles [*Tziperman et al.*, 2006]. The common feature of these two main categories is that Milankovitch forcing is not directly linked to the 100 ka timescale of the glacial-interglacial oscillations.

[4] In recent years, attention has been directed toward the tropics as a potential source for glacial cycles [e.g., *Lindzen and Pan*, 1994; *Cane*, 1998; *Clement et al.*, 1999; *Kukla et al.*, 2002; *Lea*, 2004; *Timmermann et al.*, 2007]. Several studies specifically investigated climate variability and identified an 11 ka cycle in proxy records, model simulations, and insolation records [e.g., *Short et al.*, 1991; *Hagelberg et al.*, 1994; *Lindzen and Pan*, 1994; *Berger and Loutre*, 1997; *Berger et al.*, 2006]; some of these studies related this 11 ka periodicity to the maximum equatorial insolation [e.g., *Berger et al.*, 2006]. Here we show, analytically and numerically, that the annual maximum

[1]Department of Solar Energy and Environmental Physics, The J. Blaustein Institutes for Desert Research, Ben-Gurion University of the Negev, Midreshet Ben-Gurion, Israel.
[2]Department of Environmental Sciences, Weizmann Institute of Science, Rehovot, Israel.

0883-8305/08/2007PA001436$12.00

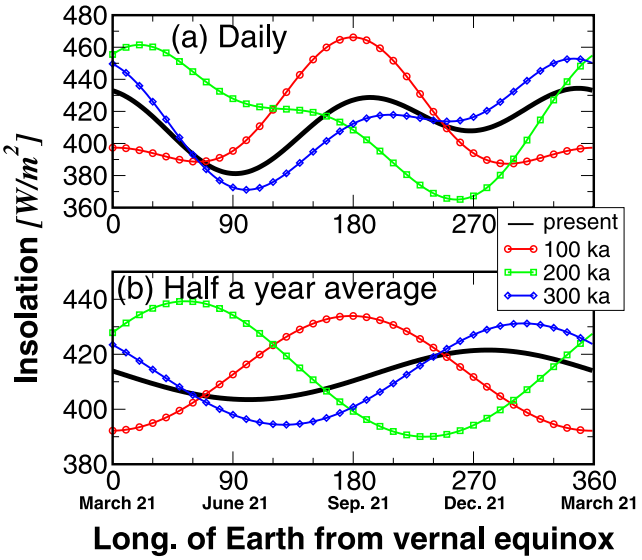

Figure 1. (a) Annual equatorial insolation curves at present, 100 ka, 200 ka, and 300 ka. Note that the pattern of the annual equatorial insolation curves changes significantly in the past where the maximum insolation can occur around the vernal or autumnal equinoxes with different amplitude. (b) Same as Figure 1a for the half a year running average insolation. See equation (14). Here, unlike the daily insolation the maximum (minimum) insolation does not necessarily occur around the vernal and autumnal equinoxes (summer and winter solstices) but can be on any date in the annual cycle. Moreover, there is only one maximum and one minimum of the half a year average insolation curves.

and minimum of equatorial insolations have a pronounced 100 ka timescale. Unlike the extra tropics for which the maximum insolation occurs very close to the summer solstice and minimum insolation occurs close to the winter solstice, the annual maximum (minimum) equatorial insolation may occur close to the one of the equinoxes (solstices). Because the equatorial ocean is a major source of heat and moisture to high latitudes [e.g., *Lindzen and Pan*, 1994; *Lea*, 2002; *Kukla and Gavin*, 2004], changes in maximum (and minimum) insolation in equatorial regions may affect development of the high-latitude continental ice sheets.

[5] The origin of the 100 ka maximum and minimum equatorial insolation periodicity can be explained briefly as follows (a detailed explanation and derivation is provided in section 2). The Sun crosses the equator twice a year, at the autumnal and vernal equinoxes. Thus, during these dates the equatorial insolation is expected to be maximal, causing subannual periodicity (Figure 1). Owing to changes in the Earth's precession, sometimes the Earth is closest to the Sun at the vernal equinox, leading to annual maximum equatorial insolation at that time, and sometimes at the autumnal equinox, leading to annual maximum equatorial insolation then. This would result in a half-precession periodicity in the annual maximum insolation of ~11 ka [*Hagelberg et al.*, 1994; *Berger and Loutre*, 1997; *Berger et al.*, 2006]. However, in addition, the distance between the Earth and the Sun varies, causing a modulation of this half-precession cycle periodicity by the eccentricity orbital parameter that has timescales of 100 and 400 ka. As a result, one would expect the maximum (and minimum) equatorial insolation to vary on timescales of half of the precession periodicity (~11 ka) and eccentricity periodicities (100 and 400 ka); below we show that the eccentricity periodicity is the dominant one.

[6] In a recent paper, *Berger et al.* [2005] discussed the origin of the 100 ka timescale in astronomical forcing; they compared several astronomical forcing parameters to various paleoclimate records. Later, *Berger et al.* [2006] showed that the difference between the maximum and minimum equatorial insolation has pronounced eccentricity frequencies and pronounced precession harmonics (mainly 5 ka periodicity). (The current study was submitted for publication before the publication of *Berger et al.* [2006]; we became aware of this paper in a late stage of the review processes.) In this study we focus on the numerical and analytical properties of the maximum and minimum equatorial insolation, both of the daily insolation and of the time-averaged insolation.

2. Equatorial Insolation: Analytical Derivations

2.1. Background

[7] Given the orbital parameters of eccentricity (e), obliquity (ε), and precession (ω), it is possible to find the daily insolation (averaged over 24 h) at a certain latitude ϕ and at a certain date within the annual cycle. The year is divided into 360 longitude degrees where a specific date in the annual cycle is associated with a certain longitude λ of the Earth on its orbit around the Sun, measured from the vernal equinox. For convenience we use the present-day dates of the equinoxes and solstices (e.g., 21 March corresponds to the vernal equinox while 21 September corresponds to $\lambda = 180$) while we note that the length of the seasons varied in past (by several days). We also note that one degree longitude does not necessarily span 24 h; see equation (11) below. The daily mean insolation is given by [*Milankovitch*, 1941; *Berger*, 1978; *Berger et al.*, 1993; *Hartmann*, 1994]

$$W = \frac{S_0}{\pi}\frac{[1+e\cos(\lambda-\omega-\pi)]^2}{(1-e^2)^2} \cdot (H_0 \sin\phi \sin\delta + \cos\phi\cos\delta\sin H_0) \quad (1)$$

where S_0 is the solar constant, δ is the declination angle given by $\sin\delta = \sin\varepsilon \sin\lambda$, and H_0 is the hour angle at sunrise and sunset given by $\cos H_0 = -\tan\phi \tan\delta$. The expression (1) is valid for latitudes $\phi < |\pi/2 - |\delta||$; above this latitude, the insolation vanishes (polar night) or is equal to $S_0 \sin\phi \sin\delta\,[1+e\cos(\lambda-\omega-\pi)]^2/(1-e^2)^2$ (polar day).

[8] At the equator $\phi = 0$, equation (1) therefore reduces to

$$W_{eq} = \frac{S_0}{\pi}\frac{[1+e\cos(\lambda-\omega-\pi)]^2}{(1-e^2)^2}\cos\delta. \quad (2)$$

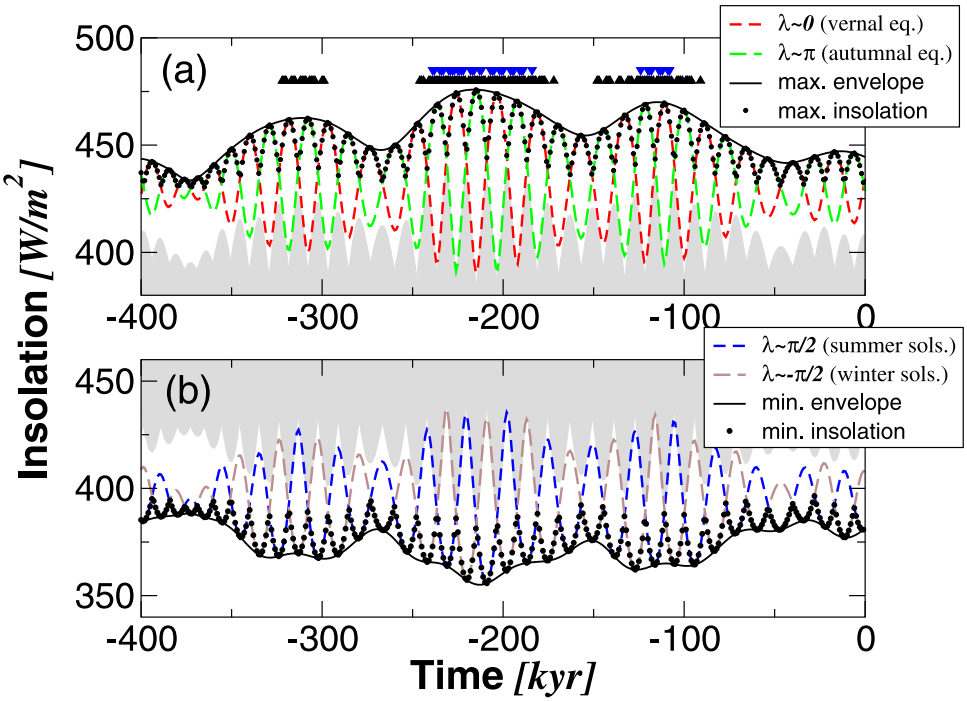

Figure 2. (a) Maximum equatorial insolation as a function of time. Black triangles pointing up represent the times for which the difference between the second maximum and the second minimum (see Figure 1) is less than 5 W/m^2; blue triangles pointing down represent the times for which there is only one maximum (and one minimum) in the annual equatorial insolation. Circles indicate the numerically constructed maximum equatorial insolation, the red and green dashed lines indicate the maximum insolation computed analytically using equations (7), (8), and (2), and the solid black line indicates the envelope of the maximum equatorial insolation as given by equation (3). (b) Minimum equatorial insolation as a function of time. Circles are the numerically constructed values, blue and brown dashed lines are the analytical approximations for minimum equatorial insolation as given by equations (9), (10), and (2), and the solid black line indicates the envelope of the minimum equatorial insolation as given by equation (4). The shaded area in Figure 2a indicates the maximum of the curves shown in Figure 2b, and the shaded area in Figure 2b indicates the minimum of the curves shown in Figure 2a. When the shaded area touches the curves (either in Figure 2a or Figure 2b), there is just one maximum and minimum in the annual cycle, since this indicates that the expected secondary minimum is equal to the expected secondary maximum and vice versa.

Our aim is to estimate the annual maximum and minimum daily insolation at the equator for a given time in the past; that is, for given orbital parameters e, ε, and ω we wish to find a specific λ that will yield the maximum (or minimum) insolation of the annual cycle.

2.2. Maximum and Minimum Equatorial Insolation: Rough Estimation

[9] The maximum insolation may be estimated by assuming $\cos(\lambda - \omega - \pi) = 1$, and that maximum equatorial insolation tends to occur around the vernal and autumnal equinoxes ($\lambda = 0, \pi$), $\cos\,\delta = 1$. The approximated maximum equatorial insolation is thus

$$W_{\mathrm{eq,max}} = \frac{S_0}{\pi(1-e)^2} \approx \frac{S_0}{\pi}(1+2e). \qquad (3)$$

The right-hand side approximation is due to the fact that $e \ll 1$. Importantly, the estimated equatorial maximum insolation depends only on the eccentricity orbital parameter that has dominant frequencies with timescales of 100 ka and 400 ka (Figure 2a).

[10] We apply a similar approach to estimate the minimal equatorial insolation within the annual cycle. To this end, we seek a λ for which equation (2) is minimum, i.e., $\cos(\lambda - \omega - \pi) = -1$, and, since minimum equatorial insolation occur around the solstices ($\lambda = \pi/2, 3\pi/2$), $\cos\,\delta = \cos\,\varepsilon$. Thus the minimum equatorial insolation may be estimated as

$$W_{\mathrm{eq,min}} = \frac{S_0 \cos\varepsilon}{\pi(1+e)^2} \approx \frac{S_0 \cos\varepsilon}{\pi}(1-2e). \qquad (4)$$

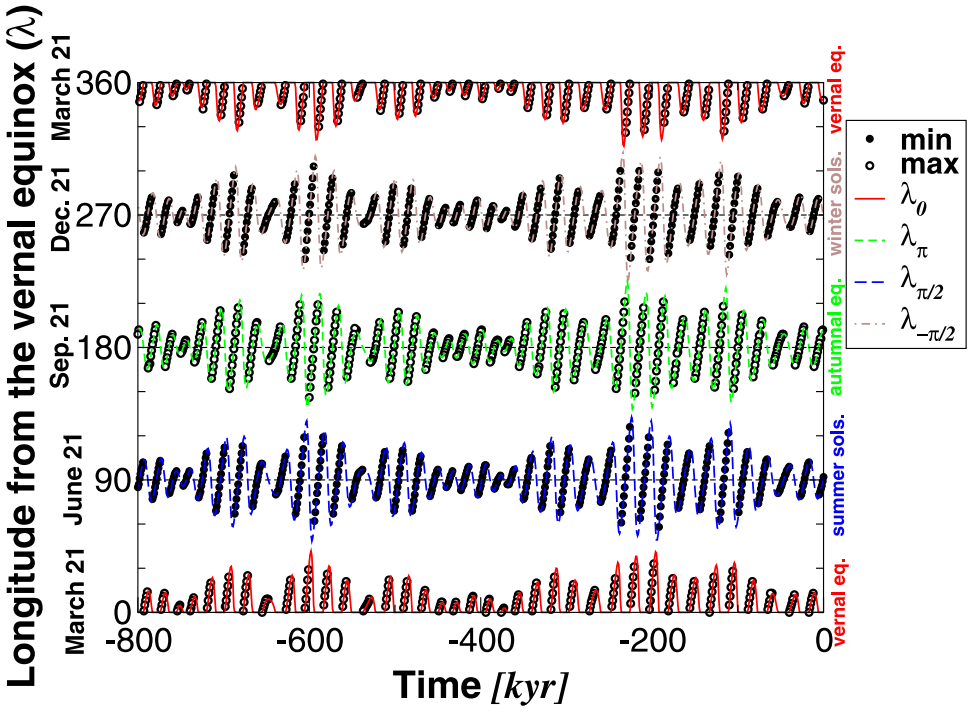

Figure 3. Longitudes of maximum and minimum equatorial insolation as a function of time. Symbols are as in Figure 2. The maximum and minimum insolations do not occur exactly at the vernal and autumnal equinoxes and at the summer and winter solstices but can occur more than 1 month before or after these dates. The analytical approximations $\lambda_{0,\pi/2,\pi,-\pi/2}$ are given by equations (7)–(10) and fit quite well the numerical results depicted by open and solid circles.

The estimated minimum equatorial insolation thus depends mainly on eccentricity but also on obliquity (Figure 2a).

[11] For typical values of S_0 = 1350 W/m^2, ε = 23.5° ($\cos\varepsilon \approx 0.92$) and $e = 0.0046$ to $e = 0.049$, the approximated maximum equatorial insolation ranges from 434 W/m^2 to 475 W/m^2, approximately 40 W/m^2 difference. This difference is large enough to influence the climate system dynamics. The minimum equatorial insolation ranges from 358 W/m^2 for $e = 0.049$ to 390 W/m^2 for $e = 0.0046$, about 30 W/m^2 difference. The difference between the maximum equatorial insolation and minimum equatorial insolation ranges from 43 W/m^2 for $e = 0.0046$ to 117 W/m^2 for $e = 0.049$; see Figures 2a and 2b.

2.3. Maximum and Minimum Equatorial Insolation: An Improved Approximation

[12] It is possible to accurately estimate the maximum and minimum equatorial insolations by taking into account the fact that the eccentricity orbital parameter and the obliquity angle are small, such that $e \ll 1$ and $\sin(\varepsilon) \approx \varepsilon$ (e is smaller than 0.05 and ε is less than 0.43 radian, 24.6°). In that case equation (2) can be approximated as

$$\tilde{W}_{\mathrm{eq}} \approx \frac{S_0}{\pi(1-e^2)^2}\left(1 - 2e\cos(\lambda-\omega) - \frac{1}{2}\varepsilon^2\sin^2\lambda\right). \tag{5}$$

The extremes can be found by differentiating equation (5) with respect to λ and equating it to zero ($\partial\tilde{W}_{\mathrm{eq}}/\partial\lambda = 0$):

$$2e(\sin\lambda\cos\omega - \cos\lambda\sin\omega) = \varepsilon^2\sin\lambda\cos\lambda. \tag{6}$$

The maximum equatorial insolation occurs around the vernal and autumnal equinoxes, $\lambda = 0$ and $\lambda = \pi$, while the minimum equatorial insolation occurs around the summer and winter solstices, $\lambda = \pi/2$ and $\lambda = 3\pi/2$. Using in equation (6) the approximations $\cos\lambda_{\lambda\approx\lambda^*} \approx \cos\lambda_* - \sin\lambda_*(\lambda - \lambda_*)$ and $\sin\lambda_{\lambda\approx\lambda^*} \approx \sin\lambda_* + \cos\lambda_*(\lambda - \lambda_*)$ for $\lambda_* = 0, \pi/2, \pi, 3\pi/2$ we obtain the following:

$$\lambda_0 = \frac{\sin\omega}{-\frac{\varepsilon^2}{2e} + \cos\omega} \quad \text{for} \quad \lambda \approx 0, \tag{7}$$

$$\lambda_\pi = \frac{\sin\omega}{\frac{\varepsilon^2}{2e} + \cos\omega} + \pi \quad \text{for} \quad \lambda \approx \pi, \tag{8}$$

$$\lambda_{\frac{\pi}{2}} = -\frac{\cos\omega}{\frac{\varepsilon^2}{2e} + \sin\omega} + \frac{\pi}{2} \quad \text{for} \quad \lambda \approx \frac{\pi}{2}, \tag{9}$$

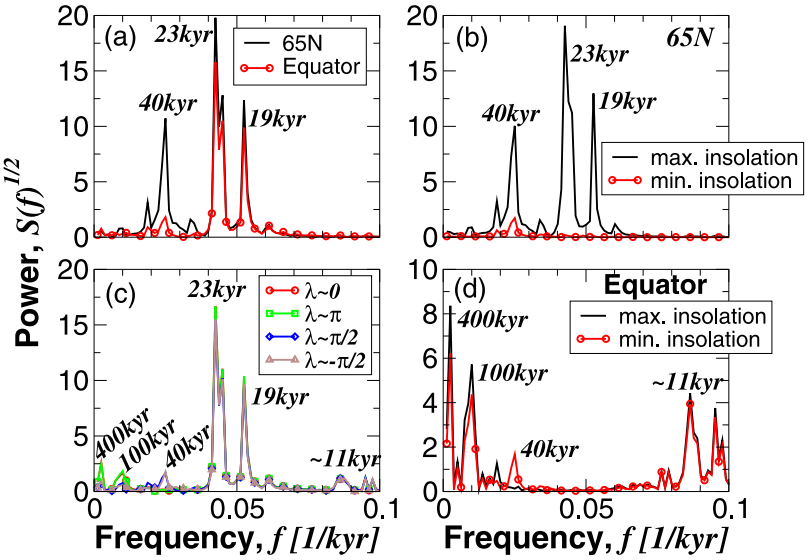

Figure 4. Power spectra of (a) 21 June 65°N and equatorial insolation, (b) maximum and minimum 65°N insolation, (c) maximum and minimum equatorial insolation near the vernal and autumnal equinoxes and near the summer and winter solstices based on equations (7)–(10) and (2), and (d) maximum and minimum equatorial insolation. Note that pronounced eccentricity periodicities are observed only in the last case.

$$\lambda_{-\frac{\pi}{2}} = -\frac{\cos\omega}{-\frac{\varepsilon^2}{2e}+\sin\omega} - \frac{\pi}{2} \quad \text{for} \quad \lambda \approx -\frac{\pi}{2}. \tag{10}$$

Once the different "dates" for the maximum and minimum insolation are approximated it is possible to insert these λ values into equation (2) to obtain the maximum and minimal equatorial insolations (see Figures 2 and 3).

[13] The annual cycle of equatorial insolation usually has two maximum and two minimum values. The expressions above provide these values at high accuracy where the insolation curves associated with these λ values have the precession periodicity (Figures 2 and 3). However, a more relevant measure may be the absolute maximum and minimum insolation in the annual cycle. In that case, for example, the longitude of the absolute maximum may switch from around the vernal equinox ($\lambda \approx 0$) to around the autumnal equinox ($\lambda \approx \pi/2$), where this switching has a periodicity of half of the precession cycle. Then, the eccentricity parameter will also be dominant, yielding pronounced 100 ka and 400 ka periodicities (Figure 4); in addition, the precession timescale will be replaced by a half-precession timescale.

2.4. Maximum and Minimum Equatorial Insolation: Time Average

[14] Heat and moisture transport from low to high latitudes are likely to influence the development of high-latitude ice sheets [*Lindzen and Pan*, 1994; *Kukla and Gavin*, 2004]. These are not likely to be dictated by a single day's insolation but rather by the average insolation over several months, a time period that can change the tropical sea surface temperature and seasonality.

[15] To evaluate the average insolation of a certain time period within the annual cycle, it is necessary to calculate (1) the time lapse between the desired longitudes (measured from the vernal equinox) based on Kepler's second law and (2) the total insolation within this time period of the annual cycle. The derivative of the time lapse, t, with respect to the longitude, λ is given by [*Milankovitch*, 1941; *Hartmann*, 1994]

$$\frac{dt}{d\lambda} = \frac{(1-e^2)^2}{\sqrt{1-e^2}} \frac{1}{(1+e\cos(\lambda-\omega-\pi))^2} \approx \left(1-e^2\right)^{3/2}(1+2e\cos(\lambda-\omega)). \tag{11}$$

The time lapse between longitude $\lambda^* - \Delta\lambda$ to $\lambda^* + \Delta\lambda$ is thus

$$T = \int_{\lambda^*-\Delta\lambda}^{\lambda^*+\Delta\lambda} \frac{dt}{d\lambda} d\lambda \approx 2\left(1-e^2\right)^{3/2}(\Delta\lambda + 2e\sin\Delta\lambda\cos(\lambda^*-\omega)). \tag{12}$$

The total insolation between longitude $\lambda^* - \Delta\lambda$ to $\lambda^* + \Delta\lambda$ using equation (2) is

$$\int_{\lambda^*-\Delta\lambda}^{\lambda^*+\Delta\lambda} W_{\text{eq}} \frac{dt}{d\lambda} d\lambda \approx \frac{S_0}{\pi\sqrt{1-e^2}} \left(2\Delta\lambda\left(1-\frac{\varepsilon^2}{4}\right) + \frac{\varepsilon^2}{4}\cos 2\lambda^* \sin 2\Delta\lambda\right). \tag{13}$$

(Note that total insolation between any two longitudes is independent of precession [e.g., *Milankovitch*, 1941; *Loutre et al.*, 2004; *Paillard*, 2001; *Huybers*, 2006]). Thus the average insolation between longitude $\lambda^* - \Delta\lambda$ and $\lambda^* + \Delta\lambda$ is

$$\overline{W}_{\mathrm{eq}} = \frac{1}{T}\int_{\lambda^*-\Delta\lambda}^{\lambda^*+\Delta\lambda} W_{\mathrm{eq}}\frac{dt}{d\lambda}d\lambda \approx \frac{S_0}{\pi(1-e^2)^2} \times \left(1+\frac{\varepsilon^2}{4}\left(\cos 2\lambda^* \frac{\sin 2\Delta\lambda}{2\Delta\lambda} - 1\right) - 2e\frac{\sin\Delta\lambda}{\Delta\lambda}\cos\left(\lambda^* - \omega\right)\right). \quad (14)$$

When $\Delta\lambda \ll 1$ (daily average insolation), equation (14) reduces to equation (5), since in that case $\sin\Delta\lambda/\Delta\lambda \to 1$.

[16] As in the previous subsection, to find the maximum and minimum of the equatorial time averaged insolation it is necessary to differentiate $\overline{W}_{\mathrm{eq}}$ with respect to λ^* and to equate it to zero ($\partial\overline{W}_{\mathrm{eq}}/\partial\lambda^* = 0$). The equation to be solved is

$$2e\frac{\sin\Delta\lambda}{\Delta\lambda}(\sin\lambda^*\cos\omega - \cos\lambda^*\sin\omega) = \varepsilon^2\frac{\sin 2\Delta\lambda}{2\Delta\lambda}\sin\lambda^*\cos\lambda^*. \quad (15)$$

This equation is similar to equation (6) and the ${\lambda^*}_{0,\pi,\pm\pi/2}$ for equation (15) are the same as in equations (7)–(10) where the factor $\frac{\varepsilon^2}{2e}$ should be replaced by $(\frac{\varepsilon^2}{2e})\cos\Delta\lambda$. Then these ${\lambda^*}_{0,\pi,\pm\pi/2}$ should be used in equation (14) to find the maxima and minima of the averaged equatorial insolation.

[17] When averaging over a longer period in the annual cycle (i.e., larger $\Delta\lambda$), the factor $\frac{\sin\Delta\lambda}{\Delta\lambda}$ becomes smaller and smaller, and thus the contribution of the precession orbital parameter in $\cos(\lambda^* - \omega)$ in equation (14) also becomes smaller. Using the average insolation over a period of several months may better represent the ocean because of its large heat capacity; the oceans act to "integrate" the effect of insolation over many days. For the special case of 6 months averaging period ($\Delta\lambda = \pi/2$), the average insolation over the time period between $\lambda^* - \pi/2$ to $\lambda^* + \pi/2$ (equation (14)) is

$$\overline{W}_{\mathrm{eq}}\left(\Delta\lambda = \frac{\pi}{2}\right) = \frac{S_0}{\pi(1-e^2)^2}\left(1 - \frac{\varepsilon^2}{4} - \frac{4e}{\pi}\cos(\lambda^* - \omega)\right). \quad (16)$$

In this case the maximum of the average equatorial insolation occurs for $\cos(\lambda^* - \omega) = -1$ (or $\lambda^* = \omega + \pi$) and is

$$\overline{W}_{\mathrm{eq,max}}\left(\Delta\lambda = \frac{\pi}{2}\right) = \frac{S_0}{\pi(1-e^2)^2}\left(1 - \frac{\varepsilon^2}{4} + \frac{4e}{\pi}\right) \approx \frac{S_0\left(1-\frac{\varepsilon^2}{4}\right)}{(1-e^2)^2(\pi - 4e)}. \quad (17)$$

The minimum of the average equatorial insolation occurs for $\cos(\lambda^* - \omega) = 1$ (or $\lambda^* = \omega$) and is

$$\overline{W}_{\mathrm{eq,min}}\left(\Delta\lambda = \frac{\pi}{2}\right) = \frac{S_0}{\pi(1-e^2)^2}\left(1 - \frac{\varepsilon^2}{4} - \frac{4e}{\pi}\right) \approx \frac{S_0\left(1-\frac{\varepsilon^2}{4}\right)}{(1-e^2)^2(\pi + 4e)}. \quad (18)$$

Unlike the daily insolation, for the half a year average equatorial insolation there is only one annual maximum and minimum where the relative phase between these two is half a year (Figure 1b). Since the Earth's position with respect to the perihelion, ν, is $\nu = \lambda - \omega - \pi$ [*Berger*, 1978; *Berger et al.*, 1993], the maximum of the half a year average equatorial insolation occurs for λ^* that coincides with the perihelion (the point on the Earth's orbit that is the closest to the Sun), while the minimum of the half a year average equatorial insolation occurs for λ^* that coincides with the aphelion (the point on the Earth's orbit that is the farthest from the Sun).

[18] Thus the maximum and minimum of the half a year average equatorial insolation depend mainly on the eccentricity orbital parameter and are independent of the precession parameter. We thus expect the maximum and minimum of the half a year equatorial insolation to have pronounced 400 ka and 100 ka timescales (eccentricity timescales), a weaker 40 ka timescale (obliquity timescale), and no ~20 ka or ~11ka timescale (semiprecession timescale) (Figures 5 and 6).

3. Equatorial Insolation: Results

[19] One of the differences between the tropics and the extratropics is that the Sun crosses the equator twice a year causing maximum insolation around the vernal and autumnal equinoxes and minimum insolation around the summer and winter solstices. On the other hand, in the NH (SH) extra tropics, maximum insolation occurs around the summer (winter) solstice while minimum insolation occurs around the winter (summer) solstice. In Figure 1a we show the equatorial annual cycle of insolation during the present, 100 ka ago, 200 ka, and 300 ka. The maximum insolation around the vernal equinox is sometimes larger than the maximum insolation around the autumnal equinox and vice versa. Moreover, in some cases there is just one maximum and minimum in the annual cycle of the equatorial insolation. This occurred, for example, 200 ka, where there was only one maximum insolation around the vernal equinox and only one minimum insolation around the winter solstice.

[20] The case of the half-year (running) average is different consistently with only one maximum and one minimum during the year. However, the maximum and minimum insolations can occur at any date in the annual cycle (see Figure 1b) in contrast to the extratropics, where they occur close to the summer and winter solstices.

[21] In order to understand more deeply the changes in the maximum equatorial insolation we show in Figure 2a (1) the

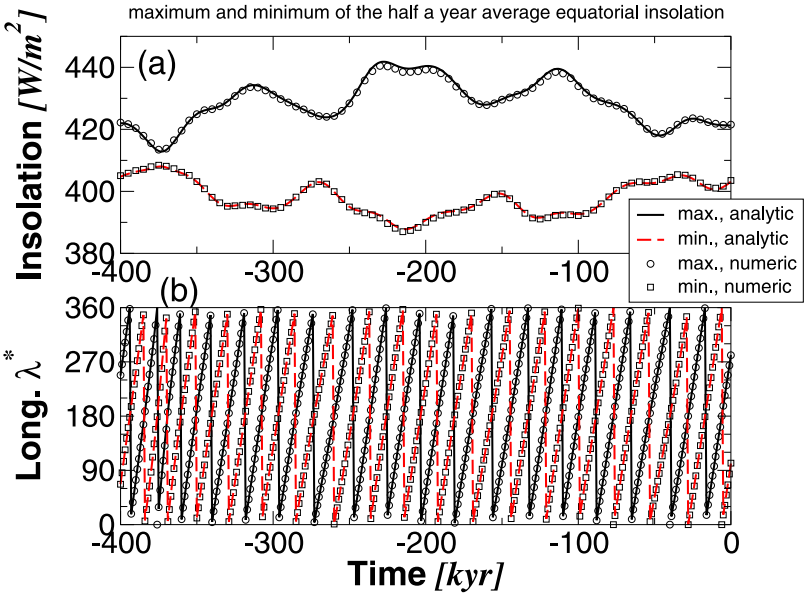

Figure 5. (a) Maximum and minimum of the half a year equatorial insolation mean. The solid and dashed lines are the approximations given by equations (17) and (18), respectively, and the circles and squares are the numerically constructed maximum and minimum values, respectively, of the half a year equatorial mean insolation. Unlike the maximum and minimum equatorial insolation that exhibits half-precession variability, here only the slow eccentricity variability is dominant. (b) Longitudes of the maximum and minimum half a year equatorial insolation mean. Symbols are as in Figure 5a. Here the dates (longitudes) at which the maximum and minimum occur span the entire annual cycle and do not necessarily occur around the equinoxes and the solstices.

numerically extracted maximal equatorial insolation curves, (2) the maximum equatorial insolation around the vernal and autumnal equinox, and (3) the ''envelope'' of the maximum insolation (equation (3)). The agreement between the ''numerically'' extracted maximum equatorial insolation and those given by equations (2), (7), and (8) is very good and supports the approximations that were assumed to derive these expressions. The maximum insolation that occurs around the vernal and autumnal equinoxes has the timescales of the precession orbital parameter (i.e., 19 and 23 ka), where these two curves have a relative phase of half of the precession cycle, approximately 11 ka. Thus, when considering just the maximal value of these two, a periodicity of ~11 ka is expected. These 11 ka cycles are modulated by the much slower frequency of the eccentricity forcing as given by equation (3) and depicted in Figure 2a. Note that the obliquity frequency of ~40 ka does not play any role here.

[22] We also plot the insolation curves of minimum insolation (Figure 2b) in a similar way to the maximum insolation which is plotted in Figure 2a. The minimal equatorial curves have similar features as the maximum equatorial curves depicted in Figure 2a. The notable difference is that the envelope of the minimal insolation has a timescale of the obliquity orbital parameter that is given by equation (4). Still, this obliquity timescale of ~40 ka is not pronounced and the dominant frequencies are that of the eccentricity (400 and 100 ka) and precession (23 and 19 ka) orbital parameters.

[23] Although the Sun crosses the equator twice a year, the equatorial insolation curves do not always have two minimum and two maximum insolation points in the annual cycles. This happens when the approximated minimum insolation given by equations (2), (9), and (10) is larger than the approximated maximum insolation given by equations (2), (7), and (8). We denoted these times by a blue triangle pointed down in Figure 2a, and it is clear that such situations occur when the eccentricity orbital parameter is large (e.g., the time period between 240 ka and 183 ka); there are 55 such points in the time interval between 400 ka to present. (When the eccentricity parameter is large, the Earth may be sufficiently far from the Sun during the equinoxes (at which the equatorial insolation is expected to be maximal), weakening the insolation compares to other dates in the annual cycle.)

[24] In Figure 3, we plot the longitudes of the Earth relative to the vernal equinox at which the maximum and minimum insolations occur. Also here the agreement between the longitudes given by equations (7)–(10) is very close to the ones numerically constructed by locating the maximum and minimum equatorial insolation from the annual insolation curves. It is also clear that the maximum equatorial insolation does indeed occur around the vernal and autumnal equinoxes while the minimum equatorial insolation occurs around the summer and winter solstices; the deviations may be as large as 1 and a half months.

[25] To demonstrate the difference between the insolation at the equatorial region and the nonequatorial regions, we

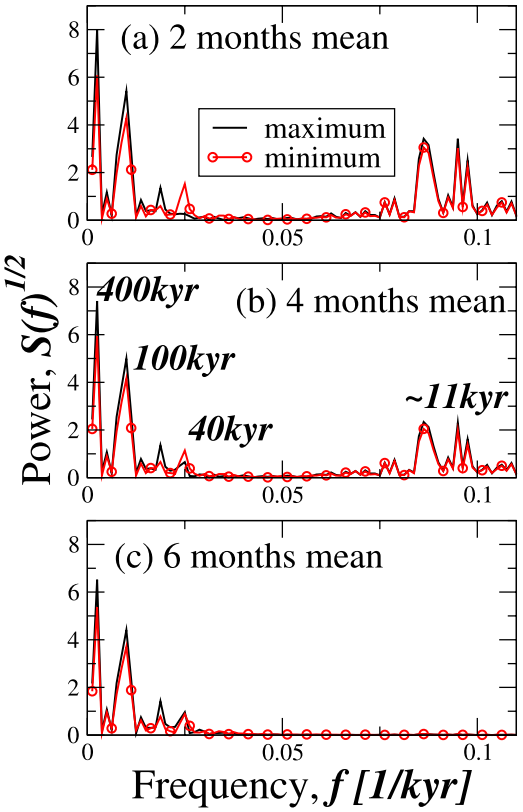

Figure 6. Power spectra of the maximum and minimum equatorial insolation for (a) 2 months mean ($\Delta\lambda = \pi/6$), (b) 4 months mean ($\Delta\lambda = \pi/3$), and (c) 6 months mean ($\Delta\lambda = \pi/2$). As the averaging period becomes larger, the half-precession periodicity (~11 ka) weakens.

plotted the power frequency spectra of different insolation curves. In Figure 4a we plotted the power spectrum of the insolation curve of the summer solstice at 65 °N and at the equator. In both curves the eccentricity frequency of 100 ka is very weak. However, while for 65°N there is a significant obliquity frequency of ~40 ka it is much weaker at the equator; note that the annual mean equatorial insolation has a dominant obliquity periodicity with variability of several W/m^2. The maximum insolation at 65°N presented in Figure 4b has almost the same power spectrum as in Figure 4a; this similarity is expected since the maximum insolation at 65°N occurs very close to the summer solstice. On the other hand, as expected, the minimum insolation at 65°N has very weak power with a dominant obliquity frequency. In Figure 4c we present the power spectra of the equatorial insolation curves given by equations (2) and (7)–(10). Also here as in Figure 4a the dominant frequency is the precession frequency; nevertheless, the frequency associated with the obliquity and eccentricity orbital parameters starts to emerge. The pronounced precession frequency is due to the oscillatory behavior of these curves as shown in Figure 2a. It is only when considering the maximum and minimum of equatorial insolation that the eccentricity frequencies become the dominant ones (Figure 4d). In this case the precession frequencies are replaced by double their values, with a timescale of ~11 ka instead of ~20 ka. The minimum equatorial insolation curve also has the obliquity frequency (equations 3 and 4).

[26] As discussed in section 2.4, if changes in equatorial maximum annual insolation impact glacial dynamics, it is more likely to be a time averaging effect. In Figure 5a we present the maximum (and minimum) of the half a year average equatorial insolation. It is notable that these curves slowly varied with timescales of the eccentricity orbital parameter, as expected from equations (17) and (18); they are somehow parallel to the envelope curves presented in Figures 2a and 2b. In Figure 5b we present the longitudes measured from the vernal equinox at which the half a year equatorial insolation is maximal and minimal. Unlike Figure 3, the maximal and minimal insolation longitudes span all longitude values and do not necessarily occur around the equinoxes and solstices. In Figure 6 we demonstrate the effect of averaging on the structure of the power spectra of the maximum and minimum insolation curves. As the averaging period becomes larger the periodicities associated with half of the precession frequencies become weaker until they totally disappear for half a year averaging (Figure 6c).

[27] Visual comparison between model and proxy data for glacial dynamics is not necessarily the right approach to validating climate models because models with very different underlying mechanisms have demonstrated a good correspondence with paleoclimate records [*Tziperman et al.*, 2006]. Still, it is possible to gain some understanding from such a comparison. In Figure 7 we present the SPECMAP δ^{18}O record [*Imbrie et al.*, 1984] (which is mainly a proxy for ice volume) together with the updated stacked benthic foraminiferal δ^{18}O record (LR04) of *Lisiecki and Raymo* [2005] and the daily (Figure 2a) and semiannual (Figure 5a) averaged maximum equatorial insolation curves. There are several observations worth noting. First the slow modulations of both proxy data and the maximum equatorial insolation curve fluctuate in a similar manner. This observation might be related to the fact that the proxy (SPECMAP) data age model is orbitally tuned to the obliquity and precession orbital parameters; the precession orbital parameter ($e \sin \omega$) also takes into account the eccentricity to which the maximum insolation seems to match. Second, the 11 ka oscillations of the daily equatorial maximum insolation are not found in the proxy data, which have precession oscillation of ~20 ka. However, other paleoclimate records do show sub-Milankovitch periodicities [*Hagelberg et al.*, 1994] although these are most probably due to the nonlinear nature of the climate system where the reported 11 ka variability is most probably an harmonic of the precession periodicity and thus most probably not related to the annual maximum daily equatorial insolation (shown in Figure 7a). On the other hand, the annual maximum of the half a year averaged equatorial insolation (shown in Figure 7b) has neither the precession periodicity nor half of the periodicity frequency. This fact suggests that maximum insolation cannot be the only force that drives glacial dynamics and that of course other processes should be considered. Third, the relatively weak maximum equa-

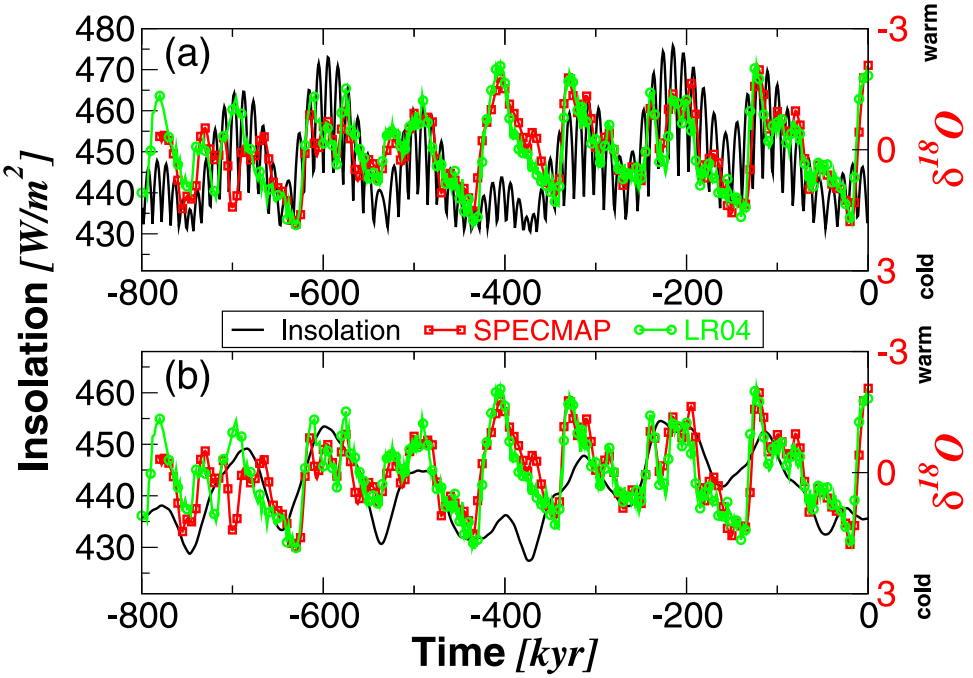

Figure 7. (a) Comparison of maximum equatorial insolation (from Figure 2a) with SPECMAP data (red line) and LR04 data [*Lisiecki and Raymo*, 2005] (green line). (b) Same as Figure 7a for the half a year mean equatorial insolation curves shown in Figure 5.

torial insolation at present and at 400 ka do not match the pronounced interglacial at that time (the so-called 400 ka problem [*Paillard*, 2001]). Forth, while glacial-interglacial oscillations are asymmetric (long glaciation followed by rapid termination), the maximum insolation curves are symmetric. All these facts suggest that even if the maximum and minimum equatorial insolations are linked to the 100 ka glacial-interglacial oscillations timescale, other processes have to be invoked to explain the characteristics of the proxy data.

4. Discussion

[28] In what ways may the variations in maximum and minimum equatorial insolation affect glacial dynamics?

[29] The precipitation-temperature feedback [*Källén et al.*, 1979; *Ghil*, 1994] suggests that the increase in accumulation rate of snow over land glaciers due to a temperature increase outweighs the corresponding increase in ablation and melting. The favorable condition will be warmer low latitudes during Northern Hemisphere winter in order to enhance evaporation, and cold conditions at high latitude so precipitation will fall as snow and not in the form of rain [*Gildor*, 2003; *Kukla and Gavin*, 2005]. Warmer low latitudes and colder high latitudes, i.e., larger meridional temperature gradient, also expect to increase the meridional moisture transport, either via increased Hadley circulation or more intense eddy activity [*Manabe and Broccoli*, 1985; *Hall et al.*, 1996; *Kukla and Gavin*, 2005; *Tziperman and Gildor*, 2003]. It is possible to try and estimate the expected effect using the results of numerous recent studies. A recent study [*Wentz et al.*, 2007] suggested an increase of a few percents in the total amount of water vapor in the atmosphere per degree of warming. Because the tropics cover half of the globe, an increase in tropical temperature resulting from an increase in maximum equatorial insolation, will lead to more evaporation and eventually more precipitation. The moisture transport depends on the intensity of the Hadley circulation and on the midlatitude eddy activity. The Hadley circulation varies seasonally where the rising motion is in the summer hemisphere with meridional transport to the winter hemisphere. The seasonal mass transport is approximately $\sim 2 \times 10^{11}$ kg/s $\approx$ 200 Sv [*Peixoto and Oort*, 1991], about 10 times larger than the Atlantic ocean meridional overturning circulation. Following *Held and Hou* [1980], *Lindzen and Hou* [1988] studied the effect of seasonality on the strength of Hadley circulation and concluded "that moving the peak heating even 2 degrees off the equator leads to profound asymmetries in the Hadley circulation, with winter cell amplifying greatly and the summer cell becoming negligible." This led *Lindzen and Pan* [1994] to associate glacial dynamics via insolation forcing to changes in the location of the maximum temperature off the equator; the precession of the equinoxes may vary the Hadley circulation intensity "by a factor of 2." Later, *Dima and Wallace* [2003] and *Walker and Schneider* [2005] suggested that the seasonal effects of the Hadley circulation are more moderate. *Hou and Lindzen* [1992] found that latitudinal heating concentration may intensify the Hadley circulation "by up to a factor of 5." The joint effect of increase in mean temperature and the meridional temperature gradient on the poleward moisture and heat transport was also estimated by *Caballero and Langen* [2005]. In the present state of

the climate system, an increase in mean temperature and/or meridional temperature gradient will significantly increase meridional heat and moisture transport.

[30] The above studies suggest that relatively small changes in the pattern of the maximum zonally averaged tropical temperature may result in drastic changes in Hadley circulation. It is plausible that as maximum equatorial insolation increases, the timing and concentration of the maximum zonally averaged temperature will change in accord, which will drastically affect the intensity of the winter cell Hadley circulation. Changes in Hadley circulation intensity may increase the midlatitude cyclone activity which acts to moderate the meridional temperature gradient and hence affects the buildup and melting of the high northern latitude ice sheets. Together with other mechanisms, the maximum equatorial insolation thus may lead to the glacial-interglacial oscillations and to the 100 ka timescale.

[31] The equatorial region plays an important role in climate dynamics and may affect glacial dynamics as well [*Cane*, 1998]. Among other phenomena unique to the equatorial region (like the El Niño) are changes in equatorial insolation. Unlike high latitudes, where maximum insolation occurs around the summer solstice and minimum insolation occurs around the winter solstice, the insolation at the equator is sometimes maximal around the vernal equinox, sometimes maximal around the autumnal equinox, sometimes with only one annual maximum and one annual minimum, and sometimes with two similar maxima and two similar minima in an annual cycle. This behavior is characterized by periodicities of 400, 100 and 11 ka. We have developed analytical expressions to describe the maximum and minimum equatorial insolation.

[32] We have also shown that when dealing with the maximum and minimum of the time averaged equatorial insolation, the half-precession periodicity becomes weaker and weaker and that it disappears for the maximum and minimum of the half a year equatorial insolation. It is more likely that the time mean equatorial insolation affects large-scale climate dynamics because SST would not respond immediately to daily insolation changes. Thus the half-precession cycle periodicity will not be pronounced in proxy records in part because of the response time of the ocean surface and in part because of other climate feedbacks.

[33] The direct effect of changing tropical insolation may be the warming or cooling of SST. This may stimulate various processes in the climate system that compete with each other and eventually cause changes in high latitudes as well. For example, the tropics, and especially the western Pacific, are a ''heat engine'' [*Lea*, 2002] and moisture source to high latitudes. The warm pool in the western equatorial Pacific has the highest SST of the ocean and is characterized by a substantial amount of warming transferred to high latitudes by atmospheric processes [*Peixoto and Oort*, 1991]. Alternation of this heat/moisture source may affect the buildup and melting of the large Northern Hemisphere (NH) continental ice sheets [e.g., *Lindzen and Pan*, 1994; *Kukla and Gavin*, 2004, 2005]. Variations in the maximum and minimum equatorial insolation may also affect ENSO and its frequency [*Cane*, 1998; *Brönnimann et al.*, 2004; *Kukla et al.*, 2002; *Kukla and Gavin*, 2005]. In addition, equatorial heat is carried to higher latitudes via the western boundary currents (the Gulf stream and the Kuroshio current) and the thermohaline (overturning) circulation. These two may affect each other through various feedback mechanisms [*Pasquero and Tziperman*, 2004]. Similarly, the monsoons, the Hadley cell circulation, and the meridional wind pattern may be changed as the maximum (and minimum) equatorial insolation changes and in this way to affect glacial dynamics. Further studies are needed to explore in more detail the potential effect of the annual maximum and minimum equatorial insolation on the climate system and on glacial dynamics.

[34] Various mechanisms have been proposed to explain the glacial-interglacial oscillations of the last 800 ka. The common feature is that the 100 ka glacial cycle is not directly caused by insolation changes. Here we suggest that the 100 ka cycle might be linked to the annual maximum and minimum equatorial insolation. Even in this case, however, other feedbacks and mechanisms have to be included in order to explain the characteristics of the glacial cycles, such as the asymmetry of glacial-interglacial oscillation (rapid deglaciation that is followed by slow glaciation) and the presence of a precession timescale in proxy records.

[35] **Acknowledgments.** We thank Gerald Dickens, David Lea, Eli Tziperman, and two anonymous reviewers for helpful discussions. This research was supported by the U.S.-Israel Binational Science Foundation. Y.A. is supported by the Israeli Center for Complexity Science. H.G. is the Incumbent of the Rowland and Sylvia Schaefer Career Development Chair.

References

Adhémar, J. A. (1842), *Révolutions de la Mer: Déluges Périodiques*, Carilian-Goeury et V. Dalmont, Paris.

Ashkenazy, Y., and E. Tziperman (2004), Are the 41 kyr glacial oscillations a linear response to Milankovitch forcing?, *Quat. Sci. Rev.*, *23*, 1879–1890.

Berger, A. (1978), Long-term variations of daily insolation and Quaternary climate changes, *J. Atmos. Sci.*, *35*, 2362–2367.

Berger, A., and M. F. Loutre (1996), Modeling the climate response to astronomical and CO_2 forcing, *C. R. Acad. Sci. Paris*, *323*, 1–16.

Berger, A., and M. F. Loutre (1997), Intertropical latitudes and precessional and half-precessional cycles, *Science*, *278*, 1476–1478.

Berger, A., M. F. Loutre, and C. Tricot (1993), Insolation of Earth's orbital periods, *J. Geophys. Res.*, *98*, 10,341–10,362.

Berger, A., J. L. Mélice, and M. F. Loutre (2005), On the origin of the 100-kyr cycles in the astronomical forcing, *Paleoceanography*, *20*, PA4019, doi:10.1029/2005PA001173.

Berger, A., M. F. Loutre, and J. L. Mélice (2006), Equatorial insolation: From precession harmonics to eccentricity frequencies, *Clim. Past*, *2*, 131–136.

Brönnimann, S., J. Luterbacher, J. Staehelin, T. M. Svendby, G. Hansen, and T. Svenoe (2004), Extreme climate of the global troposphere and stratosphere in 1940–42 related to El Niño, *Nature*, *431*, 971–974.

Caballero, R., and P. L. Langen (2005), The dynamic range of poleward energy transport in an atmospheric general circulation model, *Geophys. Res. Lett.*, *32*, L02705, doi:10.1029/2004GL021581.

Cane, M. A. (1998), Climate change: A role for the tropical Pacific, *Science*, *282*, 59–61.

Clement, A. C., R. Seager, and M. A. Cane (1999), Orbital controls on the El Niño/South-

ern Oscillation and the tropical climate, *Paleoceanography*, *14*, 441–456.
Croll, J. (1875), *Climate and Time in Their Geological Relations: A Theory of Secular Changes of the Earth's Climate*, Appleton, New York.
Dima, I. M., and J. M. Wallace (2003), On the seasonality of the Hadley cell, *J. Atmos. Sci.*, *60*, 1522–1527.
Ghil, M. (1994), Cryothermodynamics: The chaotic dynamics of paleoclimate, *Physica D*, *77*, 130–159.
Gildor, H. (2003), When Earth's freezer door is left ajar, *Eos Trans. AGU*, *84*, 215.
Gildor, H., and E. Tziperman (2000), Sea ice as the glacial cycles climate switch: Role of seasonal and orbital forcing, *Paleoceanography*, *15*, 605–615.
Hagelberg, T. K., G. Bond, and P. deMenocal (1994), Milankovitch band forcing of sub-Milankovitch climate variability during the Pleistocene, *Paleoceanography*, *9*, 545–558.
Hall, N. M. J., P. J. Valdes, and B. Dong (1996), The maintenance of the last great ice sheets: A UGAMP GCM study, *J. Clim.*, *9*, 1004–1019.
Hartmann, D. (1994), *Global Physical Climatology*, Academic, San Diego, Calif.
Held, I. M., and A. Y. Hou (1980), Non-linear axially-symmetric circulations in a nearly inviscid atmosphere, *J. Atmos. Sci.*, *37*, 515–533.
Hou, A. Y., and R. S. Lindzen (1992), The influence of concentrated heating on the Hadley circulation, *J. Atmos. Sci.*, *49*, 1233–1241.
Huybers, P. (2006), Early Pleistocene glacial cycles and the integrated summer insolation forcing, *Science*, *28*, 508–511.
Imbrie, J., J. Hays, D. Martinson, A. McIntyre, A. Mix, J. Morley, N. Pisias, W. Prell, and N. Shackleton (1984), The orbital theory of Pleistocene climate: Support from a revised chronology of the marine δ^{18}O record, in *Milankovitch and Climate*, *Part I, NATO ASI Ser., Ser. C*, vol. 126, edited by A. Berger et al., pp. 269–305, D. Reidel, Dordrecht, Netherlands.
Imbrie, J., et al. (1993), On the structure and origin of major glaciation cycles: 2. The 100,000-year cycle, *Paleoceanography*, *8*, 699–735.
Källén, E., C. Crafoord, and M. Ghil (1979), Free oscillations in a climate model with ice-sheet dynamics, *J. Atmos. Sci.*, *36*, 2292–2303.
Kukla, G., and J. Gavin (2004), Milankovitch climate reinforcements, *Global Planet. Change*, *40*, 27–48.
Kukla, G., and J. Gavin (2005), Did glacials start with global warming?, *Quat. Sci. Rev.*, *24*, 1547–1557.
Kukla, G. J., A. C. Clement, M. A. Cane, J. E. Gavin, and S. E. Zebiak (2002), Last interglacial and early glacial ENSO, *Quat. Res.*, *58*, 27–31.
Laskar, J. (1990), The chaotic motion of the solar system: A numerical estimate of the chaotic zones, *Icarus*, *88*, 266–291.
Laskar, J., F. Joutel, and F. Boudin (1993), Orbital, precessional, and insolation quantities for the Earth from −20 Myr to +10 Myr, *Astron. Astrophys.*, *270*, 522–533.
Lea, D. W. (2002), Paleoclimate: The glacial tropical Pacific–not just a west side story, *Science*, *297*, 202–203.
Lea, D. W. (2004), The 100,000-yr cycle in tropical SST, greenhouse forcing, and climate sensitivity, *J. Clim.*, *17*, 2170–2179.
Lindzen, R. S., and A. Y. Hou (1988), Hadley circulations for zonally averaged heating centered off the equator, *J. Atmos. Sci.*, *45*, 2416–2427.
Lindzen, R. S., and W. W. Pan (1994), A note on orbital control of equator-pole heat fluxes, *Clim. Dyn.*, *10*, 49–57.
Lisiecki, L. E., and M. E. Raymo (2005), A Pliocene-Pleistocene stack of 57 globally distributed benthic δ^{18}O records, *Paleoceanography*, *20*, PA1003, doi:10.1029/2004PA001071.
Loutre, M.-F., D. Paillard, F. Vimeux, and E. Cortijo (2004), Does mean annual insolation have the potential to change the climate?, *Earth Planet. Sci. Lett.*, *221*, 1–14.
Manabe, S., and A. J. Broccoli (1985), A comparison of climate model sensitivity with data from the Last Glacial Maximum, *J. Atmos. Sci.*, *42*, 2643–2651.
Milankovitch, M. (1941), *Canon of Insolation and the Ice-Age Problem* (in German), *Spec. Publ.*, vol. 132, R. Serb. Acad., Belgrade. (English translation, Israel Program for Sci. Transl., Jerusalem, 1969.)
Paillard, D. (1998), The timing of Pleistocene glaciations from a simple multiple-state climate model, *Nature*, *391*, 378–381.
Paillard, D. (2001), Glacial cycles: Toward a new paradigm, *Rev. Geophys.*, *39*, 325–346.
Pasquero, C., and E. Tziperman (2004), Effects of a wind driven gyre on thermohaline circulation variability, *J. Phys. Oceanogr.*, *34*, 805–816.
Peixoto, J., and A. Oort (1991), *Physics of Climate*, Am. Inst. of Phys., New York.
Rubincam, D. P. (2004), Black body temperature, orbital elements, the Milankovitch precession index, and the Seversmith psychroterms, *Theor. Appl. Climatol.*, *79*, 111–131.
Saltzman, B. (1987), Carbon dioxide and the δ^{18}O record of late-Quaternary climatic change: A global model, *Clim. Dyn.*, *1*, 77–85.
Saltzman, B. (1990), Three basic problems of paleoclimatic modeling: A personal perspective and review, *Clim. Dyn.*, *5*, 67–78.
Saltzman, B., and A. Sutera (1984), A model of the internal feedback system involved in Late Quaternary climatic variations, *J. Atmos. Sci.*, *41*, 736–745.
Short, D. A., J. G. Mengel, T. J. Crowley, W. T. Hyde, and G. R. North (1991), Filtering of Milankovitch cycles by Earth's geography, *Quat. Res.*, *35*, 157–173.
Timmermann, A., S. J. Lorenz, S.-I. An, A. Clement, and S.-P. Xie (2007), The effect of orbital forcing on the mean climate and variability of the tropical Pacific, *J. Clim.*, *20*, 4147–4159.
Tziperman, E., and H. Gildor (2003), The mid-Pleistocene climate transition to 100-kyr glacial cycles and the asymmetry between glaciation and deglaciation times, *Paleoceanography*, *18*(1), 1001, doi:10.1029/2001PA000627.
Tziperman, E., M. Raymo, P. Huybers, and C. Wunsch (2006), Consequences of pacing the pleistocene 100 kyr ice ages by nonlinear phase locking to Milankovitch forcing, *Paleoceanography*, *21*, PA4206, doi:10.1029/2005PA001241.
Walker, C. C., and T. Schneider (2005), Response of idealized Hadley circulations to seasonally varying heating, *Geophys. Res. Lett.*, *32*, L06813, doi:10.1029/2004GL022304.
Wentz, F. J., L. Ricciardulli, K. Hilburn, and C. Mears (2007), How much more rain will global warming bring?, *Science*, *317*, 232–235, doi:10.1126/science.1140746.

Y. Ashkenazy, Department of Solar Energy and Environmental Physics, The J. Blaustein Institutes for Desert Research, Ben Gurion University of the Negev, Sede Boqer Campus, Midreshet Ben-Gurion 84990, Israel. (ashkena@bgu.ac.il)

H. Gildor, Department of Environmental Sciences, Weizmann Institute of Science, Rehovot 76100, Israel. (hezi.gildor@weizmann.ac.il)